

13th CIRP Conference on Photonic Technologies [LANE 2024], 15-19 September 2024, Fürth, Germany

Impact of process parameters and gas atmospheres on density and microstructure of super duplex stainless steel produced by Laser Powder Bed Fusion

Michele Vanini^{a,b,c*}, Samuel Searle^{a,c}, Kim Vanmeensel^{b,†}, Bey Vrancken^{a,c,†}

^aDept. of Mechanical Engineering, KU Leuven, 3001 Leuven, Belgium

^bDept. of Materials Engineering, KU Leuven, 3001 Leuven, Belgium

^cFlanders Make@KU Leuven

†These authors contributed equally to this work and share last authorship

* Corresponding author. E-mail address: michele.vanini@kuleuven.be

Abstract

Super duplex stainless steel (2507 SDSS) is an alloy renowned for its excellent corrosion resistance and mechanical properties. This unique combination arises from a duplex microstructure characterized by austenite and ferrite. However, when processed using the laser powder bed fusion (LPBF) process, this steel contains only the ferritic phase due to the rapid cooling rates inherent in LPBF, which suppresses the formation of the austenitic phase. This study explores a parameter process optimization for this steel in two different atmospheres, Ar and N, with the latter being an austenite-stabilizing element intended to enhance the formation of the austenitic phase. A comparison of the optimal process windows between the two atmospheres is conducted, and the amount of austenitic content is evaluated as a function of the process parameters and the shielding gas employed. Findings demonstrate that utilizing a nitrogen atmosphere, in conjunction with process parameters that reduce normalized enthalpy and material evaporation, increases austenite content post-manufacture. Additionally, nitrogen as the processing gas effectively minimizes and stabilizes nitrogen content within the samples.

© 2024 The Authors. Published by Elsevier B.V.

This is an open access article under the CC BY-NC-ND license (<https://creativecommons.org/licenses/by-nc-nd/4.0/>)

Peer-review under responsibility of the international review committee of the 13th CIRP Conference on Photonic Technologies [LANE 2024]

Keywords: Laser powder bed fusion; nitrogen atmosphere; duplex stainless steel; austenite.

1. Introduction

Laser powder bed fusion (LPBF) is one of the most common additive manufacturing processes allowing the production of geometrically complex metal parts by selectively melting powder particles. With the current research trend focusing on expanding the material palette for the LPBF process, in recent years, attention has been directed towards duplex stainless steels (DSS) [1]. DSS belong to the stainless steels family and are characterized by a dual-phase microstructure containing a balanced fraction of austenite and ferrite[2]. This results in a better combination of mechanical and corrosion properties than conventional stainless steel. Super duplex stainless steels

(SDSS) are a category of DSS characterized by higher Cr and Mo concentrations [3]. However, the LPBF process of DSS and SDSS presents multiple challenges.

Tobah et al. [4] and Gargalis et al. [5] examined the density and microstructure of SDSS in relation to laser power and scan speed, noting the absence of the austenitic phase in all their samples. Mulhi et al. [6] conducted a study on density optimization, varying laser power (P), scan speed (v), and hatch distance (h). The ferrite phase fraction was observed to decrease with the decrease in energy density. This behavior was related to nitrogen evaporation during printing, caused by higher melt pool temperatures at higher energy densities. Xiang et al. [7] also observed this trend, noting an increase in austenite

content as laser power decreased. In contrast, Zhao et al. [8] and Murkute et al. [3] reported an increase in austenite content with decreased scan speed. In all the aforementioned studies, the as-built microstructure is mainly ferritic as a result of the rapid cooling inherent in the LPBF process. Consequently, a common post-processing step to achieve the desired dual phase ratio involves high-temperature annealing at around 1100°C followed by water quenching [9]. Several studies have explored methods to achieve the desired ferrite-austenite ratio directly in the as-built state. One approach involves blending SDSS powder with austenitic stainless steel 316L powder [1,10]. Another potential solution is to utilize N as a shielding gas, which has shown promising results in laser welding of DSS. The fraction of the austenite phase rose from 38% to 67% when transitioning from pure Ar shielding gas to a mixture containing N [11]. This is due to the fact that the chemical composition dictates the stability of both austenitic and ferritic phases, with the effectiveness of elements quantified through chromium equivalents (Cr_{eq}) for ferrite-stabilizing elements and nickel equivalents (Ni_{eq}) for austenite-stabilizing elements [12]. Since nitrogen has a factor of 30 in equation 1 its concentration plays a crucial role in the austenite phase fraction.

$$Ni_{eq} = Ni + 30 \times C + 30 \times N + 0.5 \times Mn \quad (1)$$

$$Cr_{eq} = Cr + Mo + 1.5 \times Si + 0.5 \times Nb \quad (2)$$

To the best of the author's knowledge, only one study has investigated the impact of the process atmosphere during LPBF on the microstructure of SDSS. Mirz et al. [12] investigated the influence of LPBF process atmosphere, specifically Ar and N, on the porosity and microstructure of SDSS. Samples produced with N atmosphere exhibited lower density and more lack of fusion and gas pores compared to those processed under argon. However, no observable difference was noted in the resultant microstructure even if the samples produced in the N atmosphere exhibited higher N concentration.

In summary, the relation between the microstructure and process parameters remains unclear since opposite trends have been observed in the literature. Additionally, the effect of laser beam diameter (d) has yet to be investigated. Moreover, although Mirz et al. [12] explored the effect of the processing atmosphere on samples produced under a specific set of process parameters, variations in laser parameters could influence melt pool lifetime and temperatures, thereby affecting the amount of nitrogen that can either evaporate from, or diffuse into the material. In this study, the porosity and microstructure of 2507 SDSS samples produced by LPBF are investigated as a function of d , P , v , and h . Samples were fabricated under both Ar and N atmospheres to assess their impact on density and microstructure. The response surface method (RSM) was adopted to optimize the experimental design and find the optimal process window.

2. Materials and Methods

2.1. Experimental setup

The present work uses a gas-atomized 2507 SDSS powder with a particle size distribution between 20 µm and 53 µm produced by m4p material solutions GmbH. The chemical composition of the powder is provided in Table 1.

Table 1. Chemical composition of the as-received powder alloys in wt%.

Cr	Cu	Fe	Mn	Mo	Ni	Si	C	N
24.8	0.02	Bal.	0.9	4.1	7.1	0.6	0.02	0.26

All the samples were manufactured using a dual laser Prima Additive Print Genius 150 LPBF machine equipped with two CS450 Series G fiber lasers, with a wavelength of 1070 nm. The printing process was conducted in Ar and N atmosphere with a constant O level of < 0.1 %. Layers were scanned using only one of the two lasers with a zigzag strategy, which was rotated 67° between each layer.

2.2. Design of experiments

Minitab v21.1 (Minitab Inc., State College, PA, USA) was used to define the RSM. RSM is a statistical technique utilized to model and analyze scenarios where multiple variables influence a response of interest, with the primary goal being the optimization of the response, i.e. the density in this specific case. Specifically, central composite design (CCD) was selected in this study, which is a common design for fitting second-order response surfaces [13]. The layer thickness was fixed to 30 µm and three d were investigated, 50 µm, 125 µm, and 200 µm. P , v , and h were optimized to maximize part density for each d . Thus, a three-factor CCD was employed for each d , which consists of 2^k factorial points, n_c center point, and $2k$ axial points, where k is the number of factors. The distance between axial points and center points (α) is set to a default value of 1.68179. The center point was replicated four times, with each replicate located in a different quadrant of the baseplate to assess the effect of building position on the part quality. The different factors investigated and their corresponding values are listed in Table 2. In total, 18 cuboids (8 mm x 8 mm x 10 mm) were generated for each d , resulting in 54 cubes per print. Furthermore, blocking was employed to determine the effect of the gas atmosphere. Blocking is a method used to analyze the impact of sources of variability on the model response and it involves grouping experiments into distinct sets, each representing specific experimental conditions. In this work, two blocks were arranged to take into account the repetition of the same job twice, under Ar and N atmosphere. The relationship between the factors and density was assessed using a second-order regression model employing the least squares method. Subsequently, analysis of variance (ANOVA), along with surface and contour plots, was utilized to evaluate the impact of each factor on the resulting density.

Table 2. Factors and corresponding values investigated at each level.

Levels	Factors		
	P (W)	v (mm/s)	h (um)
α	120	200	60
1	150	464	78
0	195	850	105
-1	240	1236	132
- a	270	1500	150

2.3. Characterization methods

The relative density of each specimen was measured using Archimedes' method. Samples with higher density, produced under different parameters, were cut in half parallel to the

building direction using wire-EDM. One half was embedded in polymer resin, ground, polished, and had its Archimedes' density verified with an optical cross-section. The same cross-section was then analyzed using a D2 Bruker X-ray diffractometer (XRD) with Cu K α radiation, employing a 0.02° step size and a 0.5-second dwell time per step. The phase quantification analysis was performed using the Rietveld refinement technique and MAUD [14] software. considering austenite fcc iron (COD 9008469) and ferrite bcc iron (COD 9008536) [1]. The other half of the samples were used to quantify nitrogen content (N wt%) with an ONH836 Elemental Analyzer.

3. Result and discussion

3.1. Process optimization

To accurately measure Archimede's density, the powder density was initially assessed using the gas pycnometry technique, yielding a density of 7.72 ± 0.01 g/cm³. This value was then employed as a reference for determining the relative density of each cube. A summary of the relative density results of the cubes produced in Ar (ρ_{Ar}) and N atmosphere (ρ_N) as a function of the process parameters is reported in Table 3. The samples analyzed by XRD are indicated in bold.

Table 3. Relative density results as a function of gas parameters and processing gas

Sample	d (μm)			50.0		125.0		200.0	
	P (W)	v (mm/s)	h (μm)	ρ_{Ar} (%)	ρ_N (%)	ρ_{Ar} (%)	ρ_N (%)	ρ_{Ar} (%)	ρ_N (%)
0	150	464	78	99.1	99.3	99.4	99.1	97.3	97.0
1	240	464	78	99.4	99.7	99.6	99.6	99.4	99.3
2	150	1236	78	97.3	97.1	93.1	91.6	89.4	89.1
3	240	1236	78	99.4	99.6	98.0	98.0	93.7	93.1
4	150	464	132	99.4	99.7	99.1	99.2	94.6	94.4
5	240	464	132	99.5	99.6	99.6	99.5	98.9	99.1
6	150	1236	132	90.0	91.0	89.0	90.3	91.4	91.7
7	240	1236	132	97.1	96.5	93.8	93.5	92.1	92.2
8	120	850	105	95.7	94.9	92.2	91.3	91.9	91.4
9	270	850	105	99.6	99.6	99.3	99.4	98.5	98.3
10	195	200	105	97.1	97.3	99.5	99.6	99.5	99.6
11	195	1500	105	94.7	94.0	91.6	91.0	91.1	89.8
12	195	850	60	99.6	99.7	97.8	98.3	94.7	94.8
13	195	850	150	97.8	97.3	94.0	94.6	91.1	91.5
14	195	850	105	99.3	99.5	98.5	98.7	92.5	92.4
15	195	850	105	99.3	99.5	98.4	98.4	93.5	92.5
16	195	850	105	99.2	99.5	98.3	98.5	93.5	92.5
17	195	850	105	99.2	99.4	98.0	98.6	94.3	93.9

By fitting the density data, three different quadratic regression models were created, one per each d investigated. The R^2 values obtained for density data acquired with d of 50 μm, 125 μm, and 200 μm are 92.5%, 95.8%, and 94.4%, respectively. The p-value test, displayed in Fig. 1., is the result of the ANOVA analysis and it indicates the significance of each coefficient used for the regression analysis. A smaller p-value corresponds to a greater influence of the respective term and typically a threshold of 0.05 to determine the significance of each term. It can be noted that the Block term does not affect the resulting relative density, independently of the d used.

Fig. 2 shows the relative density variation with respect to P and v . Fig. 2. a)-c) represent specimens with a h of 78 μm, while Fig. 2 d)-f) show those with h of 132 μm. Each set includes samples with different d : 50 μm (Fig. 2a), 125 μm (Fig. 2b), e)), and 200 μm (Fig. 2c), f)). Comparing Fig. 2 a)-c)

with 2d)-f) reveals that increased h requires lower v and higher P for consistent d . As d increases, the optimal density region shifts to higher P and lower v , due to a wider but shallower melt pool. This behavior is governed by defect mechanics governing different melting modes. A higher d spreads energy over a larger area, reducing recoil pressure and keyhole defect risks, but creates a shallower melt pool, requiring low v and high P to avoid lack of fusion porosities. In contrast, a lower d distributes energy in a smaller area, increasing the risk of evaporation and keyhole porosity at low v and high P , while too high v and low P can still lead to lack of fusion pores.

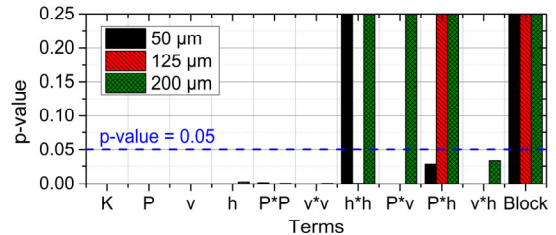


Fig. 1. P-values of each regression model term.

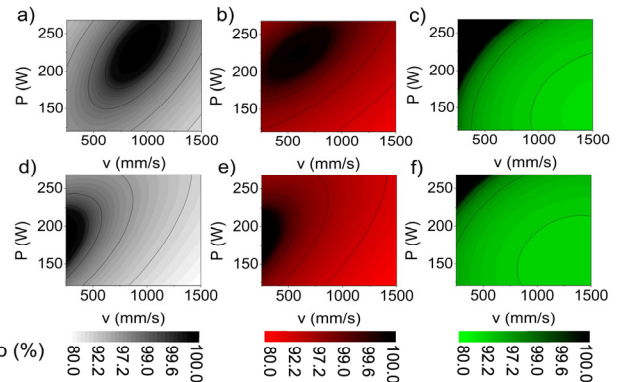


Fig. 2. Contour plot of the relative density model of the data obtained with a) $d = 50$ μm and $h = 78$ μm, b) $d = 125$ μm and $h = 78$ μm and c) $d = 200$ μm and $h = 78$ μm, d) $d = 50$ μm and $h = 132$ μm, e) $d = 125$ μm and $h = 132$ μm, and f) $d = 200$ μm and $h = 132$ μm.

3.2. Microstructure Analysis

As mentioned in Section 2.3., eight high-density samples produced under different parameters were analyzed by XRD. The XRD patterns of the selected samples are shown in Fig. 3 where the ferritic (α) and austenitic (γ) diffraction peaks can be distinguished. Each sample is labeled as (d, sample number, gas used). The diffraction peak intensities are generally similar and predominantly consist of the ferrite phase. However, the first austenitic peak (γ (111)) becomes more prominent with increasing d and decreasing v .

Fig. 4.a) and Fig. 4.b) illustrate the γ phase concentration and N wt% as a function of processing gas and normalized enthalpy (computed following [15]). The data reveal that using nitrogen gas results in a slight increase in γ phase fraction and a more stable N wt% due to the reduced nitrogen concentration gradient between the sample and the chamber atmosphere. However, the impact of process parameters on γ content is more pronounced. Generally, higher normalized enthalpy leads to a reduction in γ phase concentration. While the relationship between normalized enthalpy and N wt% is less clear, there is a general trend of decreasing N wt% with increasing

normalized enthalpy, likely due to the inverse correlation between nitrogen solubility in steel and temperature [16]. Since N stabilizes the γ phase, higher peak temperatures indirectly promote the α phase. Higher normalized enthalpy suggests a tendency toward keyhole melting, resulting in material evaporation and increased peak temperatures due to multiple laser reflections [17]. While the normalized enthalpy concept provides important information about the melting mode, it does not account for the effects of h and cooling rates. This explains why the data point (125, 10, Ar) shows very low N wt% but a higher γ content compared to (50, 1, N) and (50, 1, Ar). This behavior is the result of the combination of a moderately high normalized enthalpy and a low v leading to lower cooling rates but significant material evaporation that promotes both N depletion and γ phase formation simultaneously.

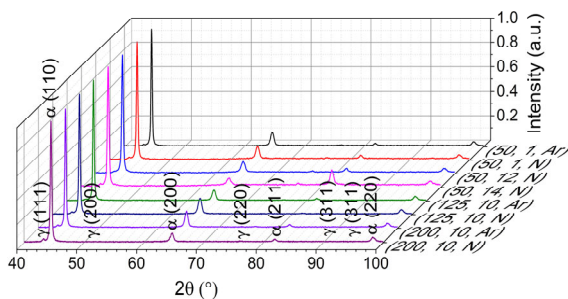


Fig. 3. XRD spectra of 2507 SDSS samples.

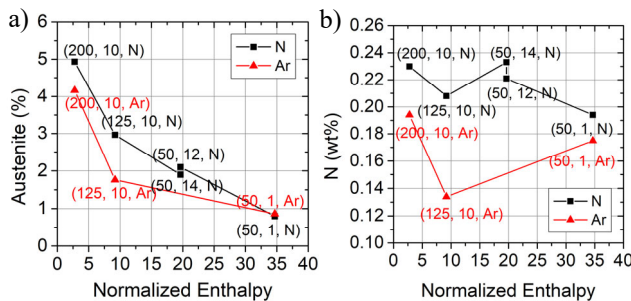


Fig. 4. Detected austenite content (a)) and N content (b)) as a function of the normalized enthalpy and processing gas.

4. Conclusions

In this research, a comprehensive process was conducted to investigate the effect of the process parameters and processing gas on the density and phase fraction of 2507 SDSS samples fabricated with LPBF process. Five main conclusions can be drawn from this study. (i) The density of the specimens was strongly affected by the processing parameters with the optimal density region moving towards lower scanning speed and higher power levels increasing the hatch spacing and laser beam diameter. (ii) The type of gas used during the process does not affect the build quality and the optimal process window. (iii) The as-built microstructure is mainly ferritic due to the high cooling rates of the LPBF process which inhibits the austenite nucleation and growth. (iv) Using nitrogen gas slightly increases the γ phase concentration, but the influence of process parameters is more significant. (v) The nitrogen atmosphere helps stabilize and retain the nitrogen content in the samples by minimizing the nitrogen concentration difference between the sample and the surrounding chamber atmosphere.

Future works will focus on a deeper understanding of the N depletion mechanism as a function of the process parameters and on the use of a dual laser LPBF machine to decrease the cooling rates and achieve the desired dual-phase microstructure in the as-built state.

Acknowledgments

This work was funded by the SIM-STREAM ICON RESONAM project under project tracking code HBC.2021.0798.

References

- [1] L. Becker et al., "Quantification of extremely small-structured ferritic-austenitic phase fractions in stainless steels manufactured by laser powder bed fusion," *Materialia (Oxf)*, vol. 22, no. December 2021, p. 101393, 2022.
- [2] K. P. Davidson and S. B. Singamneni, "Metallographic evaluation of duplex stainless steel powders processed by selective laser melting," *Rapid Prototyp J*, vol. 23, no. 6, pp. 1146–1163, 2017.
- [3] P. Murkute, S. Pasebani, and O. Burkan Isgor, "Metallurgical and Electrochemical Properties of Super Duplex Stainless Steel Clads on Low Carbon Steel Substrate produced with Laser Powder Bed Fusion," *Sci Rep*, vol. 10, no. 1, pp. 1–19, 2020.
- [4] M. Tobah, M. T. Andani, B. P. Sahu, and A. Misra, "Microstructural and Hall – Petch Analysis of Additively Steel Powder," 2024.
- [5] L. Gargalis, L. Karavias, J. S. Graff, S. Diplas, E. P. Koumoulos, and E. K. Karaxi, "A Comparative Investigation of Duplex and Super Duplex Stainless Steels Processed through Laser Powder Bed Fusion," *Metals (Basel)*, vol. 13, no. 11, 2023.
- [6] A. Mulhi, S. Dehgahi, P. Waghmare, and A. J. Qureshi, "Process Parameter Optimization of 2507 Super Duplex Stainless Steel Additively Manufactured by the Laser Powder Bed Fusion Technique," 2023.
- [7] H. Xiang, G. Chen, W. Zhao, and C. Wu, "Densification Behavior and Build Quality of Duplex Stainless Steel Fabricated by Laser Powder Bed Fusion," *Metals (Basel)*, vol. 13, no. 4, pp. 1–15, 2023.
- [8] W. Zhao, H. Xiang, R. Yu, and G. Mou, "Effects of laser scanning speed on the microstructure and mechanical properties of 2205 duplex stainless steel fabricated by selective laser melting," *J Manuf Process*, vol. 94, no. July 2022, pp. 1–9, 2023.
- [9] D. Zhang, A. Liu, B. Yin, and P. Wen, "Additive manufacturing of duplex stainless steels - A critical review," *J Manuf Process*, vol. 73, no. November 2021, pp. 496–517, 2022.
- [10] L. Gargalis, L. Karavias, J. S. Graff, S. Diplas, E. P. Koumoulos, and E. K. Karaxi, "Novel Powder Feedstock towards Microstructure Engineering in Laser Powder Bed Fusion: A Case Study on Duplex/Super Duplex and Austenitic Stainless-Steel Alloys," *Metals (Basel)*, vol. 13, no. 9, 2023.
- [11] A. B. Başyigit and A. Kurt, "The effects of nitrogen gas on microstructural and mechanical properties of TIG welded S32205 duplex stainless steel," *Metals (Basel)*, vol. 8, no. 4, pp. 1–13, 2018.
- [12] M. Mirz, S. Herzog, C. Broeckmann, and A. Kaletsch, "Influence of the L-PBF Process Atmosphere on the Microstructure and Tensile Properties of AISI 318LN Duplex Stainless Steel," *Journal of Manufacturing and Materials Processing*, vol. 6, no. 2, 2022.
- [13] D. C. Montgomery, G. C. Runger, and N. F. Hubele, *Engineering Statistics, 5th Edition*. 2010.
- [14] L. Lutterotti, "Maud: a Rietveld analysis program designed for the internet and experiment integration," *Acta Crystallogr A*, vol. 56, no. s1, pp. s54–s54, 2000.
- [15] J. Ye et al., "Energy Coupling Mechanisms and Scaling Behavior Associated with Laser Powder Bed Fusion Additive Manufacturing," *Adv Eng Mater*, vol. 21, no. 7, p. 1900185, Jul. 2019.
- [16] J. Pitkälä, L. Holappa, and A. Jokilaakso, "A Study of the Effect of Alloying Elements and Temperature on Nitrogen Solubility in Industrial Stainless Steelmaking," *Metallurgical and Materials Transactions B: Process Metallurgy and Materials Processing Science*, vol. 53, no. 4, pp. 2364–2376, 2022.
- [17] D. B. Hann, J. Iammi, and J. Folkes, "A simple methodology for predicting laser-weld properties from material and laser parameters," *J Phys D Appl Phys*, vol. 44, no. 44, 2011.